An iterative boundary potential method for the infinite-domain Poisson problem with interior Dirichlet boundaries ⋆

G. H. Miller

University of California, Department of Applied Science,
1 Shields Avenue, Davis, CA 95616.
Lawrence Berkeley National Laboratory, Applied Numerical Algorithms Group,
1 Cyclotron Road, Berkeley, CA 94720.

Abstract

An iterative method is developed for the solution of Poisson's problem on an infinite domain in the presence of interior boundaries held at fixed potential, in three dimensions. The method combines pre-existing fast multigrid-based Poisson solvers for data represented on Cartesian grids with the fast multipole method. Interior boundaries are represented with the embedded boundary formalism. The implementation is in parallel and uses adaptive mesh refinement. Examples are presented for a smooth interior boundary for which an analytical result is known, and for an irregular interior boundary problem. Second-order accuracy in L_1 with respect to the grid size is demonstrated for both problems.

Key words: Poisson problem, fast multipole method, multigrid, embedded boundary method.

1 Introduction

The Poisson problem is central to a wide variety of applications in computational physics, from electrostatics to projection methods for incompressible flow. For gridded data, or grid-mediated point data (e.g., the particle-in-cell

⋆ This work was partially supported by a contract from Capschell Inc., Chicago, IL, USA, by the US DOE MICS Division under contract number DE-FG02-03ER25579, and under subcontract B565606 with the Lawrence Livermore National Laboratory under the auspices of the Department of Energy contract No. W-7405-Eng-48.
Email address: grgmiller@ucdavis.edu (G. H. Miller).

method) the easily implemented boundary conditions are Dirichlet, Neumann, or periodic. However, for many problems the most appropriate choice, on physical grounds, is the infinite domain condition. Solutions to the infinite domain problem have been estimated using the "easy" boundary conditions in conjunction with very large computational domains, or with stretched grids, employed to remove the boundary from the region of interest. Of course such approaches are only approximate, and can be very demanding of resources especially in 3D. More rigorous boundary potential methods have been developed that determine the inhomogeneous Dirichlet conditions on a finite domain that are consistent with the desired infinite domain properties [15,13,23,1,17]. These methods exploit the free-space Green's function to construct a boundary potential from a set of screening charges.

This work is concerned with an extension of boundary potential methods to infinite domain Poisson problems that contain also surfaces with fixed potential. The solution to this combined problem is the superposition of the solution of an external Dirichlet Laplace problem (e.g., [20]) with the solution to an infinite domain Poisson problem constructed without interior boundaries. Such external Dirichlet Laplace problems involve quadrature of a codimension 1 Fredholm equation with singular kernel, integrated over the interior boundary. This results in a dense matrix equation for the charge density on the interior surface [16,20], and is similar to the capacitance matrix method of Hockney and Eastwood [8]. In 2D, the resulting matrix equation is reported to be well-conditioned for C^2 boundaries. However, the present study is concerned with 3D and C^0 boundaries where stable and accurate quadratures are not known. So, instead of pursuing this non-iterative approach an iterative method based on existing fast solvers is developed.

Consider a three dimensional rectangular domain Ω_{dom} which contains space charges prescribed through the charge density ρ, and one or more closed regions Ω_{int} with prescribed surface potentials ϕ_{int}. The objective is the solution Φ to the Poisson problem

$$\Delta\Phi = \rho \tag{1a}$$

$$\Phi = \phi_{\text{int}} \qquad \text{on } \partial\Omega_{\text{int}} \tag{1b}$$

$$\Phi(\mathbf{x}) \sim -\frac{Q}{4\pi|\mathbf{x}|} \quad \text{as } \mathbf{x} \to \infty, \tag{1c}$$

where $Q = \iiint_{\Omega_{\text{dom}}} dV\rho$.

Boundary conditions on $\partial\Omega_{\text{dom}}$ are not given explicitly, but have known properties [22]. The solution has no jump across the domain boundary,

$$[\![\Phi]\!] = 0 \qquad \text{on } \partial\Omega_{\text{dom}}, \tag{2a}$$

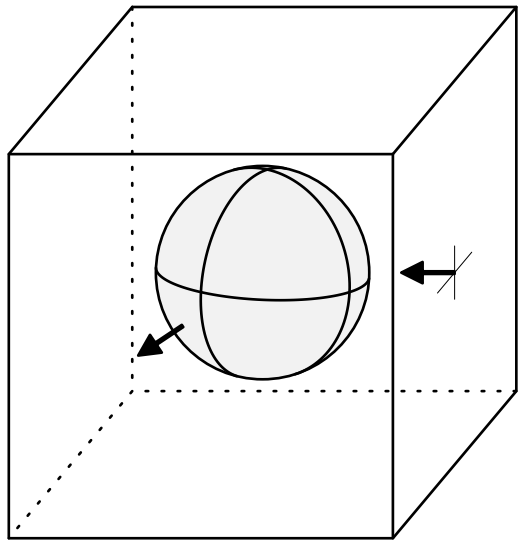

Fig. 1. Schematic view of proposed problem. The rectangular computational domain (Ω_{dom}) contains an interior object (Ω_{int}) whose surface potential ϕ_{int} is fixed. The volume $\Omega_{\text{dom}} \backslash \Omega_{\text{int}}$ may also contain a distribution of space charges ρ. Arrows signify boundary normal vectors $\mathbf{n}$.

and the surface charge density is zero,

$$[\![\mathbf{n} \cdot \nabla \Phi]\!] = 0 \qquad \text{on } \partial\Omega_{\text{dom}}. \tag{2b}$$

Here $\mathbf{n}$ is an inward-directed unit normal vector (see Fig. 1).

Alternatively, one may deduce from the uniqueness of the given problem that there exists a unique surface potential ϕ_{dom} such that the problem

$$\Delta\tilde{\Phi} = \rho \tag{3a}$$
$$\tilde{\Phi} = \phi_{\text{int}} \qquad \text{on } \partial\Omega_{\text{int}} \tag{3b}$$
$$\tilde{\Phi} = \phi_{\text{dom}} \qquad \text{on } \partial\Omega_{\text{dom}} \tag{3c}$$

has solution $\tilde{\Phi}$ which coincides with the desired solution Φ at all points interior to Ω_{dom}.

To understand ϕ_{dom}, consider its relation to the boundary potential method [15,13]. This method superimposes two solutions, the first being ϕ given by

$$\Delta\phi = \rho \tag{4a}$$
$$\phi = \phi_{\text{int}} \qquad \text{on } \partial\Omega_{\text{int}} \tag{4b}$$
$$\phi = 0 \qquad \text{on } \partial\Omega_{\text{dom}} \tag{4c}$$

in Ω_{dom}. $\phi = 0$ is the continuation of ϕ outside the domain Ω_{dom}. The homogeneous Dirichlet boundary condition on the domain boundary implies the

existence of a surface charge density ϱ_{dom}

$$\varrho_{\text{dom}} = \mathbf{n} \cdot \nabla\phi \quad \text{on } \partial\Omega_{\text{dom}}. \tag{5}$$

This boundary charge is incompatible with the condition (2b) implied by problem (1). One could correct the solution ϕ by subtracting from it the effect of the boundary charges. The correction potential is

$$\psi(\mathbf{x}) = -\iint\limits_{\partial\Omega_{\text{dom}}} d^2\mathbf{x}' G(\mathbf{x}|\mathbf{x}')\varrho_{\text{dom}}(\mathbf{x}') \quad \mathbf{x}' \text{ on } \partial\Omega_{\text{dom}}, \quad \mathbf{x} \in \Omega_{\text{dom}}, \tag{6}$$

where G is the appropriate Green's function, and $\phi+\psi$ solves (1). To appreciate the difficulty of this technique, consider the solution of (6) by establishing a boundary potential,

$$\phi_{\text{dom}}(\mathbf{x}) = -\iint\limits_{\partial\Omega_{\text{dom}}} d^2\mathbf{x}' G(\mathbf{x}|\mathbf{x}')\varrho_{\text{dom}}(\mathbf{x}') \qquad \mathbf{x}, \mathbf{x}' \text{ on } \partial\Omega_{\text{dom}} \tag{7}$$

then continuing this potential to the interior of Ω_{dom} by solving

$$\Delta\psi = 0 \tag{8a}$$
$$\psi = 0 \qquad \text{on } \partial\Omega_{\text{int}} \tag{8b}$$
$$\psi = \phi_{\text{dom}} \quad \text{on } \partial\Omega_{\text{dom}}, \tag{8c}$$

so again $\phi+\psi$ solves (1). ψ of (8) is equal to ψ of (6) provided G is the Green's function for problem (8).

Through this decomposition it is clear that the Green's function appearing in (6) and (7) cannot be the free-space Green's function,

$$G^{\text{free}}(\mathbf{x}|\mathbf{x}') = -\frac{1}{4\pi|\mathbf{x}-\mathbf{x}'|}, \tag{9}$$

because boundary condition (8b) is not enforced by G^{free}. The boundary potential method in the absence of interior boundaries [15,13] uses the free space Green's function. An analogous technique for problem (1) would require a different Green's function.

The correct Green's function is constructed through consideration of induced surface charges. A unit space charge density at $\mathbf{x}'$ will create a potential everywhere on $\partial\Omega_{\text{int}}$. An induced surface charge density must be present on the surface $\partial\Omega_{\text{int}}$ whose effect is to zero the potential on that boundary. $G(\mathbf{x}|\mathbf{x}')$ must therefore relate the space charge density at $\mathbf{x}'$ to the measurement point $\mathbf{x}$, and must also account for the effect of all induced charges:

$$G(\mathbf{x}|\mathbf{x}') = G^{\text{free}}(\mathbf{x}|\mathbf{x}') + \iint\limits_{\partial\Omega_{\text{int}}} d^2\mathbf{x}'' G^{\text{free}}(\mathbf{x}|\mathbf{x}'')\tilde{\varrho}_{\text{int}}(\mathbf{x}''|\mathbf{x}'), \tag{10}$$

where $\tilde{\varrho}_{\text{int}}(\mathbf{x}''|\mathbf{x}')$ is the induced surface charge density at $\mathbf{x}''$ due to the unit space charge density at $\mathbf{x}'$. $\tilde{\varrho}_{\text{int}}$ is determined by applying condition (8b) to (10), evaluated on the interior boundary:

$$0 = G^{\text{free}}(\mathbf{x}|\mathbf{x}') + \iint\limits_{\partial\Omega_{\text{int}}} d^2\mathbf{x}'' G^{\text{free}}(\mathbf{x}|\mathbf{x}'')\tilde{\varrho}_{\text{int}}(\mathbf{x}''|\mathbf{x}') \qquad \forall \mathbf{x} \text{ on } \partial\Omega_{\text{int}}. \tag{11}$$

Numerical quadrature of (11) leads to the capacity matrix method [8] and the boundary integral methods after Mayo and Rokhlin [16,20].

Consideration of (7) with (10) indicates that the boundary potential ϕ_{dom} could be calculated if the induced interior boundary surface charge density ϱ_{int} were known. Conversely, by analogy to (5) the solution to problem (8) provides ϱ_{int} given ϕ_{dom}. The combination of these two observations yields an iterative scheme for the determination of ϕ_{dom}. This algorithm is stated below in §2, and demonstrated through an analytical example in §3. In section §4 the established numerical methods used to implement the algorithm are described briefly. Second-order accuracy in L_1 for C^∞ and C^0 interior boundaries is demonstrated in §5.

2 Algorithm

The iterative algorithm proceeds as follows.

I. First, solve the homogeneous Dirichlet domain boundary problem

$$\Delta\phi = \rho \tag{12a}$$
$$\phi = \phi_{\text{int}} \quad \text{on } \partial\Omega_{\text{int}} \tag{12b}$$
$$\phi = 0 \quad \text{on } \partial\Omega_{\text{dom}}. \tag{12c}$$

II. Second, compute the charge density on the domain boundary and compute an estimated boundary potential by utilizing the free space Green's function. The superscript in parenthesis will denote an iteration index.

$$\varrho_{\text{dom}} = \mathbf{n}\cdot\nabla\phi \quad \text{on } \partial\Omega_{\text{dom}}. \tag{13a}$$
$$\phi^{(0)}_{\text{dom}}(\mathbf{x}) = -\iint\limits_{\partial\Omega_{\text{dom}}} d^2\mathbf{x}' G^{\text{free}}(\mathbf{x}|\mathbf{x}')\varrho_{\text{dom}}(\mathbf{x}'). \tag{13b}$$

Now proceed with iteration index $k = 1$.

III. Compute the induced charge on the interior boundary. This proceeds by first solving the Laplace problem (8)

$$\Delta\psi^{(k)} = 0 \tag{14a}$$

$$\psi^{(k)} = 0 \qquad \text{on } \partial\Omega_{\text{int}} \tag{14b}$$
$$\psi^{(k)} = \phi_{\text{dom}}^{(k-1)} \qquad \text{on } \partial\Omega_{\text{dom}}, \tag{14c}$$

where $\psi^{(k)}$ is taken to be zero everywhere within Ω_{int}. The induced surface charges are then

$$\varrho_{\text{int}}^{(k)} = \mathbf{n} \cdot \nabla\psi^{(k)} \qquad \text{on } \partial\Omega_{\text{int}}. \tag{15}$$

IV. These induced surface charges modify the boundary potential,

$$\phi_{\text{dom}}^{(k)}(\mathbf{x}) = \phi_{\text{dom}}^{(0)}(\mathbf{x}) + \iint\limits_{\partial\Omega_{int}} d^2\mathbf{x}' G^{\text{free}}(\mathbf{x}|\mathbf{x}')\varrho_{\text{int}}^{(k)}(\mathbf{x}'). \tag{16}$$

V. If the boundary potential has converged, the iteration ceases and $\Phi = \phi + \psi^{(k)}$. Convergence is assessed by measuring the L_2 norm of $|\phi_{\text{dom}}^{(k)} - \phi_{\text{dom}}^{(k-1)}|$. Otherwise, $k := k + 1$ and recompute the induced charge (Step III).

If this algorithm converges, then the domain boundary potential (16) is consistent with the modified Green's function (10), i.e., (16) is equivalent to

$$\phi_{\text{dom}}(\mathbf{x}) = -\iint\limits_{\partial\Omega_{\text{dom}}} d^2\mathbf{x}' G(\mathbf{x}|\mathbf{x}')\varrho_{\text{dom}}(\mathbf{x}'). \tag{17}$$

The behavior and convergence properties of the algorithm can be shown with a small analytical example. In §3 it will be shown that the algorithm outlined above will fail to converge when the interior boundary and domain boundary are close (in a sense that will be made clear). One remedy for this convergence problem is to replace (16) with

$$\phi_{\text{dom}}^{(k)}(\mathbf{x}) = \omega\phi_{\text{dom}}^{(0)}(\mathbf{x}) + \omega \iint\limits_{\partial\Omega_{int}} d^2\mathbf{x}' G^{\text{free}}(\mathbf{x}|\mathbf{x}')\varrho_{\text{int}}^{(k)}(\mathbf{x}') + (1-\omega)\phi_{\text{dom}}^{(k-1)}(\mathbf{x}) \tag{18}$$

for $0 < \omega < 1$. (18) has the same stationary point as (16) and enables convergence for essentially any well-resolved geometry where Ω_{int} is contained within Ω_{dom}.

3 Analytical Example

For an analytical exposition in 3D it is convenient to use spherical geometry. Let Ω_{dom} be a sphere of radius $a > 1$, and let Ω_{int} be a concentric sphere of radius 1, and omit space charges ρ. The potential can at all times be expanded in spherical harmonics. With three simple observations, the analytical example

is easily carried out: (i) the spherical harmonic modes are fully decoupled from one another; (ii) the ℓm spherical harmonic component of the potential varies with r like $\alpha r^l + \beta r^{-(\ell+1)}$; and (iii) if the ℓm component of charge density on a spherical shell of radius r_1 is ϱ_ℓ^m, then the potential due to this charge density has amplitude $\phi_\ell^m = -\frac{r_1^{\ell+2}}{r_2^{\ell+1}}\frac{\varrho_\ell^m}{2\ell+1}$ evaluated on a spherical shell with radius $r_2 \geq r_1$.

Let ϕ_{int} have amplitude f_ℓ^m in harmonic mode ℓm. The solution to algorithm step I is

$$\phi_\ell^m(r,\theta,\phi) = f_\ell^m \frac{\left(\frac{r}{a}\right)^\ell - \left(\frac{a}{r}\right)^{\ell+1}}{\left(\frac{1}{a}\right)^\ell - \left(\frac{a}{1}\right)^{\ell+1}}. \tag{19}$$

Associated with this solution is the domain surface charge density ϱ_{dom} and associated domain surface compensating potential, step II:

$$\varrho_{\text{dom}}{}_\ell^m = -\frac{f_\ell^m}{a}\frac{(2\ell+1)}{\left(\frac{1}{a}\right)^\ell - \left(\frac{a}{1}\right)^{\ell+1}} \tag{20a}$$

$$\phi_{\text{dom}}^{(0)}{}_\ell^m = -f_\ell^m \frac{1}{\left(\frac{1}{a}\right)^\ell - \left(\frac{a}{1}\right)^{\ell+1}}. \tag{20b}$$

The general solution to the Laplace problem of step III is

$$\psi^{(k)}{}_\ell^m = \phi_{\text{dom}}^{(k-1)}{}_\ell^m \frac{\left(\frac{r}{1}\right)^\ell - \left(\frac{1}{r}\right)^{\ell+1}}{\left(\frac{a}{1}\right)^\ell - \left(\frac{1}{a}\right)^{\ell+1}}, \tag{21a}$$

and the corresponding induced surface charge on the interior boundary is

$$\varrho_{\text{int}}^{(k)}{}_\ell^m = \phi_{\text{dom}}^{(k-1)}{}_\ell^m \frac{(2\ell+1)}{\left(\frac{a}{1}\right)^\ell - \left(\frac{1}{a}\right)^{\ell+1}} \tag{21b}$$

giving a new boundary potential, step IV:

$$\phi_{\text{dom}}^{(k)}{}_\ell^m = \phi_{\text{dom}}^{(0)}{}_\ell^m - \phi_{\text{dom}}^{(k-1)}{}_\ell^m \frac{1}{a^{2\ell+1}-1}. \tag{22}$$

The sequence (22) converges to

$$\phi_{\text{dom}}^{*}{}_\ell^m = \phi_{\text{dom}}^{(0)} \frac{a^{2\ell+1}-1}{a^{2\ell+1}} = f_\ell^m \frac{a^\ell}{a^{2\ell+1}-1} \tag{23}$$

provided $a^{2\ell+1} > 1$. The 00 mode is the slowest to converge, requiring $a > 2$. The same conclusion regarding the 00 mode may be drawn through analysis

of [12, problem 1.6]. The converged correction field ψ_ℓ^m (21), added to the initial calculation ϕ_ℓ^m (18), gives the exact analytic result Φ_ℓ^m for the model problem:

$$\Phi_\ell^m(r,\theta,\phi) = f_\ell^m r^{-(\ell+1)}. \tag{24}$$

With the relaxed convergence scheme of (18), algorithm step IV would give

$$\phi_{\mathrm{dom}\ell}^{(k)\ m} = \omega\phi_{\mathrm{dom}\ell}^{(0)\ m} - \omega\phi_{\mathrm{dom}\ \ell}^{(k-1)m}\frac{1}{a^{2\ell+1}-1} + (1-\omega)\phi_{\mathrm{dom}\ \ell}^{(k-1)m} \tag{26}$$

in place of (22). This sequence converges to (23) for

$$0 < \omega < 2\left[1 - a^{-(2\ell+1)}\right]. \tag{28}$$

If a space charge density were included in this example, the potential fields ϕ and Φ would differ from the formulae given above by addition of the convolution $G * \rho$, where the particular Green's function used here maintains zero potential on the interior sphere. A particularly efficient solution is given by the method of images [12, §2.4].

4 Implementation

The numerical method uses a Cartesian grid finite volume approach with cell-centered data. Complex interior geometries are represented by overlaying the interior domain on the Cartesian grid. Cut cells are characterized by volume fraction, cell surface area fractions, and an interface normal vector. The implementation is built using the `Chombo` library of block-structured data management and operation tools [5, p. 273]. The treatment of complex geometry is based on ideas in [14], and has been developed for hyperbolic, parabolic, and elliptic problems in [4,18,21].

4.1 Poisson solvers

Algorithm steps I and III solve Dirichlet boundary condition Poisson problems using the second-order accurate approach of [21]. The approach uses a divergence form of the Laplace operator, with cell-edge fluxes at irregular domains being computed through specialized high-order stencils. Geometric multigrid is employed, with graph-based coarsening operators making possible coarse-grid relaxation at resolutions below which the interior geometry may be resolved. Additional detail on the stencil operations may be found in [19].

4.2 Boundary charge calculation

Domain boundary charges (algorithm Step II) are estimated using a one-sided finite difference approximation to $\mathbf{n} \cdot \nabla\phi$. When adaptive mesh refinement is used estimates of surface charge may be available at several grid resolutions. In that case the values computed at the highest resolution are used, and underlying coarse cell approximations are discarded.

Charges computed on the interior boundary (algorithm Step III) are estimated in each cell containing an interface. The derivative $\mathbf{n} \cdot \nabla\phi$ is obtained by solving a least squares problem for the first derivatives, second derivatives, and the second-order cross derivative terms of ϕ. The centering point of the Taylor series is the centroid of the intersection of the interior boundary with the computational cell. This least squares problem uses data from all "regular" cells (cells that do not contain an interface and are not contained inside the interior boundary), and that are in a line of sight with the cell in which the gradient is desired. This last condition eliminates from the least squares fit those data that are "close", but which may be separated from the centering point by thin boundary walls. The least squares problem is solved by Householder QR reduction, and the result is stored as a stencil – a set of pairs of weights and cell coordinates. The relatively expensive stencil construction occurs once in the method, and each iterative evaluation of algorithm Step III involves a computationally inexpensive evaluation of the stencil. The interior boundary surface charge in a cell is proportional to the product of the derivative $\mathbf{n} \cdot \nabla\phi$ with the area of the interior boundary. As with domain boundaries, with adaptive mesh refinement the charge may be computed at multiple resolutions. The values used are obtained at the finest available level of resolution.

4.3 Free space Green's functions

Algorithm steps II and IV involve computing domain boundary potentials from surface charge densities. The free-space Green's function convolution is solved using an implementation of the fast multipole method (FMM) [7,6,3], which follows closely the non-adaptive scheme presented in [6] [1]. The rotation of multipole and local expansions make use of rotation matrices constructed by the very efficient recursive method of Ivanic and Ruedenberg [10,11] [2].

The FMM calculates local expansions which represent the potential in a neighborhood from charges well-separated from that neighborhood. Charges that

[1] The imaginary exponent in [6, Eq. (7.17)] and [3, Eq. (49)] should be negative. [7, Eq. (3.60)] is correctly rewritten as [6, Eq. (5.6)] and [3, Eq. (17)].
[2] Table 2 is correct in [10] not [11].

are not well-separated are evaluated by direct calculation, $-1/4\pi|\mathbf{r}|$. When calculating the domain boundary potential due to domain boundary charges, it is necessary to account for the case where the charge and potential are co-located. This is accomplished using an integral formulation for the potential at a point due to a uniform charge density over a 2D square source (e.g., [9, Eqs. (4-6)]). All domain potentials computed directly from domain charges make use of this strategy. If ever an interior boundary charge need to be transfered directly to an domain boundary potential, a point-to-point $-1/4\pi|\mathbf{r}|$ calculation is used, the points being respective centroids.

The FMM uses a hierarchy of Cartesian data layouts on a cubic domain. The finest level of FMM refinement corresponds with a coarsened version of the Poisson domain, suitably extended to be cubic and have length be a power of 2. The coarsening is not essential, but improves performance by balancing the cost of multipole→local operations against the number of direct $-1/4\pi|\mathbf{r}|$ operations required.

When adaptive mesh refinement is used, the boundary potential is calculated on all available levels of refinement that abut $\partial\Omega_{\text{dom}}$.

5 Results and Conclusions

The first example verifies the method by comparing calculations against analytical solutions. The interior boundary is a sphere of radius 0.1, centered in a cubic domain of length 1, resembling the cartoon of Fig. 1. A collection of 200 point charges surround the sphere. Their coordinates are chosen randomly to lie inside the torus with major radius 0.2 and minor radius 0.05, bisected by the horizontal midplane of the sphere. The sphere has fixed potential with 00 and 22 spherical harmonic modes (using the real part with Greengard's choice of normalization), with magnitude 1 and 10, respectively. The spherical coordinates are rotated relative to the cube in order to break the symmetry of the problem, via $R_z(45°) \circ R_y(15°) \circ R_z(30°)$. The analytic reference solution for the potential due to the sphere is treated in a straightforward manner. The Cartesian grid representation of the analytic contribution of the point charges is more delicate. In each computational cell, an analytical volume average of the $-1/4\pi|x|$ potential is calculated for the given charges and for the image charges used to respect the interior boundary condition. For the numerical solution, the point charges are distrubuted on the grid using a cloud-in-cell distribution [2]. Second order convergence in L_1 is found (Table 1). In L_∞ the convergence is $\mathcal{O}(h^1)$: an inherent problem of particle-in-cell type methods. With the point charges omitted, the corresponding Laplace problem is second-order accurate in all norms (Table 2)

Table 1
Convergence study for sphere with 200 point charges. Errors are based on analytical formulas.

$1/h$	L_∞	rate	L_1	rate	L_2	rate
16	$0.151\ 10^2$		$0.175\ 10^1$		$0.209\ 10^1$	
32	$0.341\ 10^1$	2.14	$0.145\ 10^0$	3.60	$0.158\ 10^0$	3.73
64	$0.171\ 10^1$	1.00	$0.337\ 10^{-1}$	2.10	$0.381\ 10^{-1}$	2.05
128	$0.829\ 10^0$	1.04	$0.734\ 10^{-2}$	2.20	$0.100\ 10^{-1}$	1.93

Table 2
Convergence study for sphere without point charges. Errors are based on analytical formulas.

$1/h$	L_∞	rate	L_1	rate	L_2	rate
16	$0.129\ 10^2$		$0.113\ 10^0$		$0.189\ 10^0$	
32	$0.335\ 10^1$	1.95	$0.132\ 10^{-1}$	3.10	$0.438\ 10^{-1}$	2.11
64	$0.126\ 10^1$	1.41	$0.389\ 10^{-2}$	1.76	$0.123\ 10^{-1}$	1.83
128	$0.237\ 10^0$	2.41	$0.799\ 10^{-3}$	2.29	$0.248\ 10^{-2}$	2.31

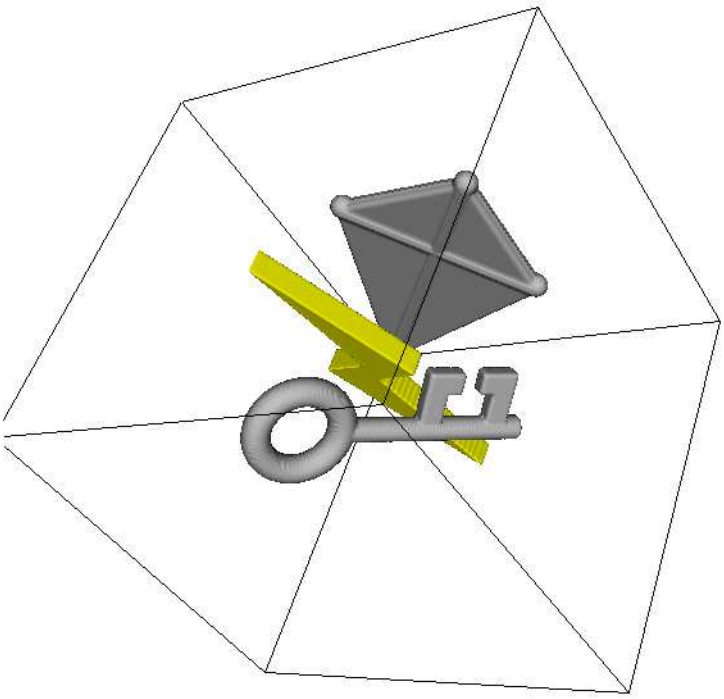

Fig. 2. Geometry of second test: Franklin's experiment with a bolt of charge.

The second example demonstrates the robustness of the method by showing second order convergence for a case where the interior boundaries are not smooth. The interior surface is C^0 on a set of codimension 2, and C^∞ elsewhere. In some cells containing these C^0 regions a sufficiently large stencil of points is not always available for a second-order computation of the interior boundary charge. However, since the set of such points is only codimension 2, the overall solution displays second-order convergence in L_1. The interior boundaries are held at fixed potential $\phi_{\text{int}} = 0$, and a C^0 distribution of space charges ρ is prescribed (Fig. 2). Because of the proximity of the interior boundaries to the domain boundary, relaxation is used with $\omega = 0.7$. The convergence results (Table 3) are second-order in L_1 and L_2. A rate of order h^0 is found for L_∞: this is the expected result for C^0 boundaries in L_∞ for Poisson's problem with the embedded boundary formalism [21, §2.2].

Table 3
Convergence study for C^0 geometry. Errors are based on Richardson extrapolation.

$1/h$	L_∞	rate	L_1	rate	L_2	rate
16 vs. 32	$0.231\ 10^{-1}$		$0.273\ 10^{-3}$		$0.365\ 10^{-3}$	
32 vs. 64	$0.745\ 10^{-3}$	1.63	$0.394\ 10^{-4}$	2.78	$0.407\ 10^{-4}$	3.17
64 vs. 128	$0.292\ 10^{-3}$	1.35	$0.171\ 10^{-4}$	1.22	$0.174\ 10^{-4}$	1.22
128 vs. 256	$0.289\ 10^{-3}$	0.015	$0.335\ 10^{-5}$	2.36	$0.342\ 10^{-5}$	2.35

Although the spatial extent of the FMM grid hierarchy (§4.3) may be larger than the Poisson domain, ϕ and ψ are not computed on the extended domain. In this sense the present method is very compact. In contrast, the methods of [13] and [17] solve fast (FFT-based) Poisson problems on extended domains as part of their boundary potential calculation. Note that the method presented here, applied to a problem with no interior domain, solves the same problem as [13,17], non-iteratively ($\Phi = \phi + \psi^{(0)}$), on a compact domain.

The method presented here may be adapted to solve the infinite domain Poissom problem with Neumann boundary conditions on the interior domain. Three changes are required: (i) ϕ of step I would have an inhomogeneous Neumann condition on the interior surface; (ii) $\psi^{(k)}$ of step III would have a homogeneous Neumann condition on the interior boundary; and (iii) the induced charge distribution on the interior boundary would be a double layer. Across a double layer the jump in $\partial\psi/\partial\mathbf{n}$ is zero, thus the potential inside the interior domain is constant. By application of the divergence theorem, with there being no charges in Ω_{int}, it follows that the constant must be zero. Finally, the jump in potential across a double layer gives σ [22, L.15 §2]. With the interior value of ψ being zero,

$$\sigma(\mathbf{x}_0) = \lim_{x \to \mathbf{x}_0} \frac{-\psi(\mathbf{x})}{4\pi}, \qquad \mathbf{x}_0 \text{ on } \delta\Omega_{\text{int}}, \tag{30}$$

where the limit is approached from the outside the interior domain. The Green's function used to compute the change in boundary potential $\phi_{\text{dom}}^{(k)}$ due to the double layer is the negative of the normal derivative of the free space Green's function. The FMM method is easily adapted to this case [7].

Acknowledgements

GHM thanks P. Colella, D. T. Graves, and D. Trebotich for many insightful discussions.

References

[1] G. T. Balls and P. Colella. A finite difference domain decomposition method using local corrections for the solution of Poisson's equation. *J. Comp. Phys.*, 180:25–53, 2002.

[2] C. K. Birdsall and D. Fuss. Clouds-in-clouds, clouds-in-cells physics for many-body plasma simulation. *J. Comp. Phys.*, 3:494–511, 1969.

[3] H. Cheng, L. Greengard, and V. Rokhlin. A fast adaptive multipole algorithm in three dimensions. *J. Comp. Phys.*, 155:468–498, 1999.

[4] P. Colella, D. T. Graves, B. J. Keen, and D. Modiano. A Cartesian grid embedded boundary method for hyperbolic conservation laws. *J. Comp. Phys.*, 211:347–366, 2006.

[5] W. Gibson. *Spook Country.* Putnam, New York, 2007.

[6] L. Greengard and V. Rokhlin. A new version of the fast multipole method for the Laplace equation in three dimensions. *Acta Numerica*, 6:229–269, 1997.

[7] L. F. Greengard. *The Rapid Evaluation of Potential Fields in Particle Systems.* MIT Press, Cambridge, MA, 1988.

[8] R. W. Hockney and J. W. Eastwood. *Computer Simulation Using Particles.* McGraw-Hill, New York, 1981.

[9] G. Hummer. Electrostatic potential of a homogeneously charged square and cube in two and three dimensions. *J. Electrostatics*, 36:285–291, 1996.

[10] J. Ivanic and K. Ruedenberg. Rotation matrices for real spherical harmonics. Direct determination by recursion. *J. Phys. Chem.*, 100:6342–6347, 1996.

[11] J. Ivanic and K. Ruedenberg. Additions and corrections. *J. Phys. Chem. A*, 102:9099–9100, 1998.

[12] J. D. Jackson. *Classical Electrodynamics.* Wiley, New York, 2nd edition, 1975.

[13] R. A. James. The solution of Poisson's equation for isolated source distributions. *J. Comp. Phys.*, 25:71–93, 1977.

[14] H. Johansen and P. Colella. A Cartesian grid embedded boundary method for Poisson's equation on irregular domains. *J. Comp. Phys.*, 147:60–85, 1998.

[15] K. Lackner. Computation of ideal MHD equilibria. *Comp. Phys. Comm.*, 12:33–44, 1976.

[16] A. Mayo. The fast solution of Poisson's and the biharmonic equations on irregular regions. *SIAM J. Num. Anal.*, 21:285–299, 1984.

[17] P. McCorquodale, P. Colella, G. T. Balls, and S. B. Baden. A local corrections algorithm for solving Poisson's equation in three dimensions. *Comm. App. Math. and Comp. Sci.*, 2:57–81, 2007.

[18] P. McCorquodale, P. Colella, and H. Johansen. A Cartesian grid embedded boundary method for the heat equation on irregular domains. *J. Comp. Phys.*, 173:620–635, 2001.

[19] A. Nonaka, D. Trebotich, G. H. Miller, D. T. Graves, and P. Colella. A higher-order upwind method for viscoelastic fluids. *Comm. App. Math. and Comp. Sci.*, 2007. in prep.

[20] V. Rokhlin. Rapid solution of volume integral equations of classical potential theory. *J. Comp. Phys.*, 60:187–207, 1985.

[21] P. Schwartz, M. Barad, P. Colella, and T. Ligocki. A Cartesian grid embedded boundary method for the heat equation and Poisson's equation in three dimensions. *J. Comp. Phys.*, 211:531–550, 2006.

[22] S. L. Sobolev. *Partial differential equations of mathematical physics.* Pergamon, Oxford, 1964.

[23] Z. J. Wang. Efficient implementation of the exact numerical far-field boundary condition for Poisson equation on an infinite domain. *J. Comp. Phys.*, 153:666–670, 1999.